Transport in Porous Media (2005) 60:225–240
DOI 10.1007/s11242-004-5738-z

Numerical Simulation of a CT-Scanned Counter-Current Flow Experiment

G. LI[1,*], Z. T. KARPYN[2], P. M. HALLECK[2], and A. S. GRADER[2]
[1]*Petroleum Engineering Department, University of Tulsa, Keplinger Hall, Room L125, 600 South College Ave, Tulsa, OK 74104-3189, U.S.A.*
[2]*Petroleum and Natural Gas Engineering Program, Pennsylvania State University, Hosler Building, University Park, PA 16802, U.S.A.*

(Received: 22 October 2003; accepted in final form: 2 November 2004)

Abstract. Counter-current flow occurs in many reservoir processes and it is important to understand and model these processes in order to operate them effectively. Both drainage and imbibition processes exist simultaneously during counter-current flow. It has thus proven difficult to model this type of flow using conventional techniques because of the impossibility of assigning a single capillary pressure curve applicable over the entire sample. In the current paper, a new saturation-history-dependent approach has been developed to simulate a counter-current flow experiment done with an X-ray CT scanner. Hysteresis in both capillary pressure and relative permeabilities is considered during simulation. Capillary hysteresis loop and relative permeabilities are extracted through history matching and a family of scanning curves is constructed connecting the two branches of the capillary hysteresis loop. Each gridblock of the sample is assigned a different scanning curve according to the local saturation history. History-dependent modeling of the experiment reproduced two-dimensional saturation distributions over time with good accuracy, which cannot be obtained with traditional simulation using only one capillary pressure curve.

Key words: counter-current flow, hysteresis, scanning curves, history matching.

Nomenclature

a_i, b_i	coefficients in power form relative permeability equation of phase i.
$a_{\mathrm{pc}}, b_{\mathrm{pc}}$	coefficients in capillary pressure equation based on vertical saturation profile.
F	weighing factor in Killough hysteresis capillary pressure equation.
g	gravity acceleration constant.
J	objective function for optimization.
k	permeability.
k_r	relative permeability.
k_{ri}	relative permeability of phase i.
p_c	capillary pressure.
p_c^*	function of final vertical saturation profile.

*Tel.: +918-6312426; Fax: +918-6312059; e-mail: gaoming-li@utulsa.edu

p_c^d the bounding drainage capillary pressure.
p_c^i the bounding imbibition capillary pressure.
$p_{c\mathrm{REV}}^d$ drainage capillary pressure value at the saturation reversal point.
S_g gas saturation.
S_g^i gas saturation corresponding to an imbibition capillary pressure value.
S_{gr} residual gas saturation.
$S_{g\mathrm{REV}}$ gas saturation where the saturation reversal occurs.
S_i phase i saturation.
S_{ir} residual phase i saturation.
$S_{x,y,z,t}^{\mathrm{calc}}$ calculated saturation from the simulator at location (x, y, z) of the sample and time t.
$S_{x,y,z,t}^{\mathrm{exp}}$ saturation from the experiment at location (x, y, z) of the sample and time t.

Greek symbols

$\nu_{\mathrm{w}}, \nu_{\mathrm{nw}}$ wetting and non-wetting phase flow velocity, respectively.
$\rho_{\mathrm{w}}, \rho_{\mathrm{nw}}$ wetting and non-wetting phase density.
$\lambda_{\mathrm{w}}, \lambda_{\mathrm{nw}}$ wetting and non-wetting phase mobility.
λ_{te} total effective mobility.
ε curvature parameter in Killough hysteresis capillary equation.
Ω range of the saturation data.

1. Introduction

Gravity-driven counter-current flow in porous media is encountered in many environmental processes such as groundwater contamination and decontamination, and rainwater percolation in soil. It also occurs in many petroleum reservoir processes such as primary and secondary migration of hydrocarbons, gas storage in aquifers, and steam-assisted-gravity drainage. Another good example is the recovery process of attic oil. Attic oil is defined as the crude oil located at the top of a reservoir, above the structurally highest well. The most frequent reason for uneconomical extraction of the remaining attic oil is that water has risen to the level of the well resulting in a high water-cut. The amount of attic oil normally does not justify the expense of drilling another well in this zone, so the attic oil cannot be produced by conventional technology. A huff-and-puff (simplified as H-n-P) recovery technique is usually applied to recover the remaining attic oil. In this technique, the well with the highest elevation is used for both injection and production. It is a cyclic process and follows three steps in each cycle: (1) gas is injected (Huff); (2) the well is shut in to allow gas migrate up and form a gas cap; (3) the well is then re-opened and put back on production (Puff). During the shut-in period, gas migrates up and oil flows down towards the well, which is a counter-current flow process driven by gravity in a closed system. The understanding of the mechanisms of counter-current flow helps the implementation of these recovery processes.

Early experiments in gravity-driven counter-current flow in a closed system were done by Templeton *et al.* (1962), and by Briggs and Katz (1966). In both experiments, drainage and imbibition flow regimes were observed simultaneously. Because of the co-existence of drainage and imbibition in such systems, the attempt by Briggs and Katz (1966) to simulate their experiments with only one imbibition capillary pressure curve reproduced unsatisfactory saturation profiles. On the other hand, if both drainage and imbibition capillary pressure curves were used, there would be a discontinuous transition zone between the two regimes.

The specific experiment studied in this paper was performed by Barbu *et al.* (1999). The 51-mm sample was made of glass beads. There were two mobile phases, benzyl alcohol and decane, and one immobile phase, water. An X-ray CT scanner was used to quantify saturation distributions in the sample. There were two main stages in this counter-current flow experiment. In stage 1, with an initially homogeneous saturation distribution, the mobile fluids (benzyl alcohol and decane) segregated due to gravity. Benzyl alcohol (heavy phase) moved down and decane (light phase) moved up. Figure 1(a) shows the progressional saturation distributions during this stage. Dark color represents high benzyl alcohol saturation while light color represents high decane saturation. To initiate stage 2, the sample was rotated 180°. Benzyl alcohol and decane then exchanged places, again driven by gravity. Figure 1(b) shows the progressional saturation distributions during stage 2.

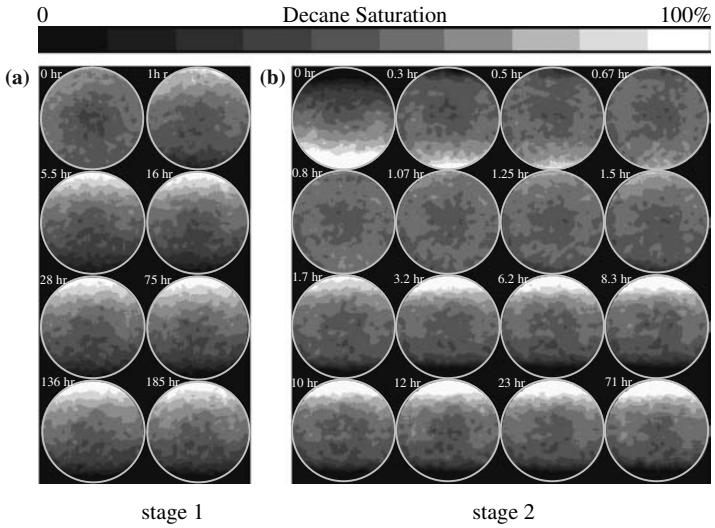

Figure 1. Saturation distribution during Barbu *et al.*'s counter-current flow experiment.

Al-Wadahi *et al.* (2000) studied the above experiment with a neuro-simulation approach. In their study, one pair of relative permeability curves was represented with a power form shown in Equation (1).

$$k_{ri} = a_i \, (S_i - S_{ir})^{b_i} \tag{1}$$

where S_i is the phase i saturation and S_{ir} is the residual phase i saturation. a_i and b_i are parameters to be determined. The capillary pressure curve was generated based on the vertical final saturation profile as in Equation (2).

$$p_c = a_{\text{pc}} p_c^* + b_{\text{pc}} \tag{2}$$

where $p*_c$ is a function of final fluid saturation distribution obtained from experiments and the constants a_{pc} and b_{pc} are parameters to be determined. The constants, and thus the relative permeability and capillary pressure curves for the experiments, were determined with a well-trained Artificial Neural Network (ANN).

With one pair of relative permeability curves and a single S-shaped capillary pressure curve (termed as single p_c method in this study), simulation by Eclipse® only reproduces the general behavior of the two-dimensional saturation distributions, as shown in the bottom row of Figure 2. This simplified method, using a single capillary pressure curve, recreates a smoothed version of the actual saturation distributions. These simulated saturation distributions are strongly affected by the shape of the sample, which is not seen from the experimental data in the top row of Figure 2.

We believe that the limitation in the early attempts at modeling counter-current flow processes is a result of neglecting the co-existence of drainage and imbibition, and the hysteresis in capillary pressure and relative permeabilities. The objective of the present work is to improve understanding of counter-current flow by modeling the processes with a newly developed modeling approach that includes these previously neglected factors.

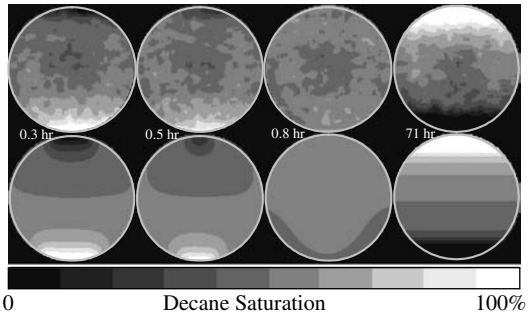

Figure 2. Comparison of saturation distribution between the experiment (top row) and the single p_c simulation (bottom row).

2. Capillary Pressure and Hysteresis

Capillary pressure may exhibit hysteresis. According to both experimental observation and Everett's independent domain theorems (Everett, 1967; Morrow 1970), capillary pressure is characterized with a closed loop consisting of the bounding imbibition and drainage curves, and intermediate "scanning" curves. When the process starts at an end point (irreducible or maximum saturation), it follows a bounding capillary pressure curve. When direction of saturation change reverses before reaching the end point, the process follows a capillary pressure scanning curve.

Figure 3 shows the general behavior of capillary hysteresis with the loop of drainage and imbibition capillary pressure curves and the scanning curves for both drainage and imbibition processes (Morrow and Harris, 1965). The thick solid lines are the bounding curves and dots connected with thin lines are the experimental scanning curves. Figure 3a shows the imbibition-scanning curves. These curves depart abruptly from the bounding drainage capillary pressure curve, and then descend toward the bounding imbibition capillary pressure curve approaching it asymptotically. Figure 3b shows the drainage-scanning curves. These curves start at points on the bounding imbibition capillary pressure curve and asymptotically approach the bounding drainage capillary pressure curve. The behaviors of bounding drainage and imbibition capillary pressure curves and the

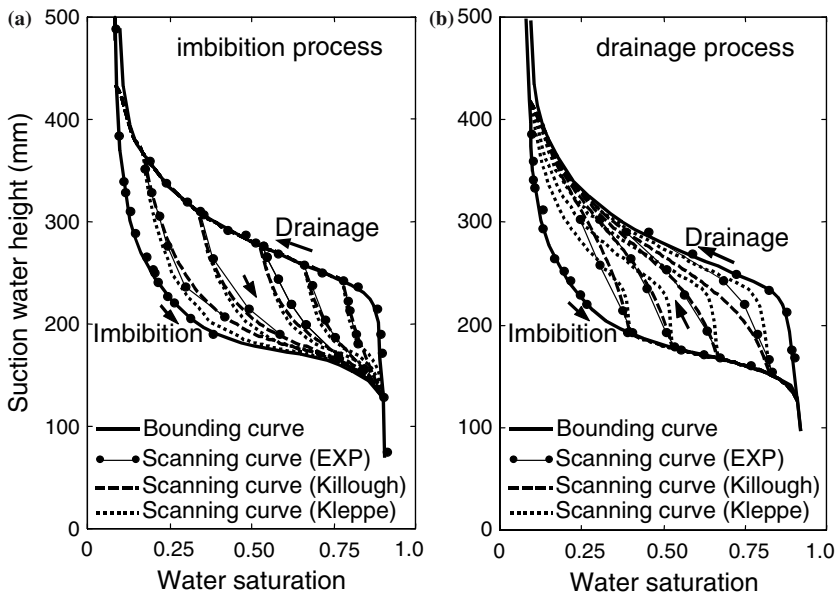

Figure 3. Capillary pressure hysteresis loop and scanning curves: experiments (from Morrow and Harris, 1965) and modeling from Kleppe *et al.* and Killough methods.

corresponding scanning curves are consistent with Everett's independent domain theory, which requires the scanning curves converge tangentially onto the bounding curves.

In the following, we are going to examine some existing methods used to construct scanning curves in the literature. From Poulovassilis' study (1962), the drainage-scanning curves can be constructed if the primary imbibition-scanning curves are known from experiments and *vice versa*. Philip (1964) reexamined the independent domain theory with the similarity hypothesis. In his method, the scanning curves can be constructed with only the hysteresis loop. With a predetermined normalized density distribution function, the hysteresis loop can be completed from only one branch (drainage or imbibition) and hence the family of scanning curves can be approximated.

Although the above methods for constructing scanning curves are based on fundamental physical models, they are not convenient to apply to reservoir modeling. Killough (1976) and Kleppe *et al.* (1997) have proposed some models for capillary pressure scanning curves, and these models can be readily incorporated into reservoir modeling. In the following, Killough and Kleppe *et al.* methods are briefly stated.

The method presented by Killough (1976) predicts hysteresis capillary pressure by using weighted average of the complete drainage and imbibition curves. For an oil-gas system, his formula for an imbibition-scanning curve initiated from the bounding drainage curve may be written as:

$$p_c = p_c^d + F\left(p_c^i - p_c^d\right) \tag{3}$$

where the superscripts d and i represent drainage and imbibition, respectively and the same convention holds for the all the other equations in the paper. The weighting factor F is defined as:

$$F = \frac{\frac{1}{S_{g\mathrm{REV}} - S_g + \varepsilon} - \frac{1}{\varepsilon}}{\frac{1}{S_{g\mathrm{REV}} - S_{gr} + \varepsilon} - \frac{1}{\varepsilon}} \tag{4}$$

The function F depends only on the point where the p_c leaves the bounding curve and on a predetermined interpolative parameter for the curvature, ε. The usual range for ε is 0.05–0.1 according to Killough (1976). S_g is the current gas saturation. $S_{g\mathrm{REV}}$ is where the saturation reversal occurs and S_{gr} is the residual gas saturation. A similar expression is used for imbibition-scanning curves.

The Kleppe *et al.* method (1997) is based on the strong similarity between the scanning curves and the corresponding bounding curves of the hysteresis loop. An imbibition-scanning curve initiated on the bounding drainage capillary pressure curve at $S_g = S_{g\mathrm{REV}}$ and ending at $S_g = S_{gr}$ may be defined as:

$$p_c\left(S_g\right) = p_c^i\left(S_g^i\right) \tag{5}$$

where S_g^i the gas saturation corresponding an imbibition capillary pressure value and defined as,

$$S_g^i = S_{gr} + \left[\frac{S_g^i\left(p_c^i = p_{c\mathrm{REV}}^d\right) - S_{gr}}{S_{g\mathrm{REV}} - S_{gr}}\right]\left(S_g - S_{gr}\right) \tag{6}$$

applicable in the saturation range: $S_{g\mathrm{REV}} \geq S_g \geq S_{gr}$. $p_{c\mathrm{REV}}^d$ is the drainage capillary pressure value at the saturation reversal point. $S_g^i\left(p_c^i = p_{c\mathrm{REV}}^d\right)$ is the gas saturation where the imbibition capillary pressure value p_c^i equals $p_{c\mathrm{REV}}^d$. Basically, Equations (5) and (6) scale the imbibition capillary pressure curve in the interval between S_{gr} and $S_g^i\left(p_c^i = p_{c\mathrm{REV}}^d\right)$ to the imbibition scanning curve in the interval between S_{gr} and $S_{g\mathrm{REV}}$.

A similar process is applied to drainage-scanning curves initiated on the imbibition capillary curve.

Figure 3 also shows the comparison of the scanning curves constructed by these two methods and the match with the experiment from Morrow and Harris (1965). The dashed lines represent the scanning curves from Killough method and the dotted lines from Kleppe *et al.* method. There is a good match between constructed imbibition-scanning curves from both methods and the experimental data shown in Figure 3(a). In Figure 3(b), the drainage-scanning curves from Killough method have a better match than these from Kleppe *et al.* method. The interpolative parameter ε in Killough method is 0.1. In the following analysis, we used Killough method to generate drainage-scanning curves and Kleppe et al. method to generate imbibition-scanning curves.

3. History-Dependent Modeling

Early attempts (Briggs and Katz, 1966; Al-Wadahi *et al.*, 2000) to simulate counter-current flow experiments used one capillary pressure curve and one pair of relative permeability curves. Simulation attempts using either drainage or imbibition capillary pressure curves failed to reproduce the counter-current flow experiments. Using the single p_c method, Al-Wadahi *et al.* (2000) simulated Barbu *et al.*'s (1999) experiments with limited success. The capillary pressure curve was constructed based on the final saturation profile and it was then adjusted using a neuro-simulation method to match experiment. The obtained capillary pressure curve is S-shaped, which could not be explained. However, we will show below that simulations using conventional capillary pressure curves but taking into account capillary hysteresis and local saturation history can account for the apparent behaviors. According to Everett's independent domain theory (Everret, 1967),

any point within a hysteresis loop can be reached by many paths. The path by which the point is attained must be specified to get a complete description of the status of the system (Morrow, 1970).

A detailed description on how capillary pressure changes temporally and spatially during gravity driven counter-current flow is presented next. In this case, heavy and light phases are the wetting and non-wetting phases, respectively, which is consistent with the actual experiment. Drainage will occur with increment of light phase saturation, while imbibition will occur with increment of heavy phase saturation. In the experiment, the sample is first drained by continuous injection of light non-wetting phase following the capillary pressure path AO in Figure 4(c), until a homogeneous saturation distribution is obtained. Note that this step is done when the core is placed in a vertical direction to avoid gravity segregation. This homogeneous distribution is denoted in the vertical saturation profile, Figure 4(a), by the "initial" dashed line with constant non-wetting phase saturation (S_{nw}). At this point, the system is closed allowing fluids to segregate due to density difference. As the light phase migrates upwards, drainage will take place in the upper portion of the sample, following the drainage capillary pressure curve along path OB (Figure 4(c)). Simultaneously, as the heavy phase migrates downwards, imbibition will occur in the lower portion of the sample, following the imbibition capillary pressure curve along path OA (Figure 4(c)). At the end of this segregation process (stage 1), there will be high non-wetting phase saturation at the top of the sample and low non-wetting phase saturation at the bottom, denoted by the solid "Final" line in Figure 4(a), A′O′B′.

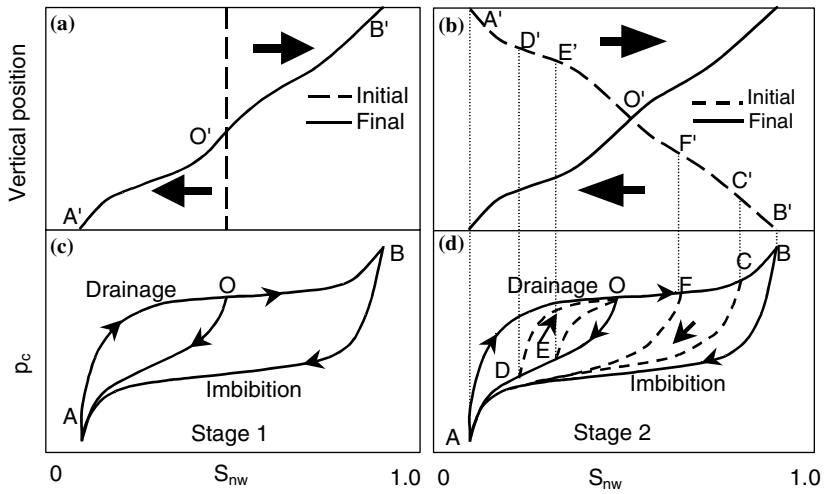

Figure 4. Schematic of history-dependent modeling.

The sample is then rotated 180°, forming the initial condition for stage 2. The initial saturation profile in this stage is shown in Figure 4(b) by the "initial" dashed line A′O′B′. The upper and lower portions of the sample will again undergo drainage and imbibition processes, respectively. In this case, capillary pressures in the upper portion of the sample are located on the OEDA capillary pressure curve (Figure 4(d)) at initial conditions. Thus, the segregation process will follow drainage-scanning curves such as DO and EO. The corresponding initial saturations are points D′ and E′ on the initial vertical saturation profile in Figure 4(b). Simultaneously, capillary pressures in the lower portion of the sample are located on the bounding drainage capillary pressure curve OB (Figure 4(c)) at initial conditions. Thus, the segregation process will follow imbibition-scanning curves such as CA and FA. The corresponding initial saturations are points C′ and F′ on the initial vertical saturation profile. The end points, A′ and B′, on the initial vertical saturation profile will follow the bounding drainage and imbibition capillary pressure curves, respectively. The final saturation profile for segregation stage 2 is denoted by the solid line in Figure 4(b).

From the above discussion, the model will need to take capillary pressure hysteresis and local saturation history into account. In history-dependent modeling, different capillary pressure (scanning) curves are assigned to different locations according to their initial saturation and saturation history, and different relative permeability curves are assigned to the different flow regimes. In the experiment studied, the upper part of the sample undergoes a drainage flow regime and is assigned with drainage-scanning curves and a pair of drainage relative permeability curves. The lower part of the sample undergoes an imbibition flow regime and is assigned with imbibition-scanning curves and a pair of imbibition relative permeability curves.

4. Automatic-History-Matching Method

Our history-dependent modeling method requires two pairs of relative permeability curves and the bounding curves of the capillary hysteresis loop. However, none of these curves were available for modeling. An automatic-history-matching method was applied to extract these parameters from the experimental data.

The forward model for automatic-history-matching is a commercial reservoir simulator (Eclipse®). With a diameter of 51 mm of the core sample, we partitioned the circular cross section of the sample with a 79 by 79 Cartesian grid and there is one only layer along the core sample with a thickness of 8.467 mm. The edge of the sample in the simulation is approximated with a zigzag curve and the cells outside of the edge are

treated as inactive cells in the Eclipse input file. The simulation time steps are tuned to accommodate the experimental time steps shown in Figure 1.

The objective function for optimization is expressed as the squared difference between the simulation and experimental saturation distributions in the following form:

$$J = \sum_{\Omega(x,y,z,t)} \left(S^{\text{calc}}_{x,y,z,t}(k_r, p_c) - S^{\text{exp}}_{x,y,z,t} \right)^2 \tag{7}$$

where $S^{\text{calc}}_{x,y,z,t}$ is the calculated saturation distribution in the sample, which is a function of relative permeability k_r and capillary pressure p_c. Relative permeabilities and capillary pressures are adjusted to minimize the objective function J until the process converges. The following describes the optimization process incorporated with history-dependent modeling:

(1) Set initial guess for relative permeabilities and capillary pressure hysteresis loop.
(2) Generate capillary pressure scanning curves according to the initial saturation and local saturation history for each gridblock.
(3) Enter the relative permeabilities and capillary pressures together with other properties (porosities, absolute permeabilities, etc.) into the reservir simulator.
(4) Use the simulator to obtain the spatial and temporal saturation maps.
(5) Compare the experimental data (saturation distributions) and the simulation results, and calculate the objective function J.
(6) If the objective function is within a tolerance, the relative permeabilities and capillary pressures have been found; otherwise the relative permeabilities and capillary pressures are automatically adjusted and start a new iteration.

During the history matching process the reservoir simulator is treated as a subroutine. For each iteration, the useful information (saturation distributions of the sample) is extracted from the simulation output and used for optimization, and then the simulation input is updated using the optimized model parameters (relative permeability and capillary pressure curves).

During this research, three optimization algorithms were tested: Steepest Descent method, Gauss Newton method, and Levenburg–Marquardt method. The Steepest Descent method is stable but too slow to be applied to a large system. The Gauss Newton method is fast, but unstable if the iteration step size is large. The Levenburg–Marquardt method can be viewed as a combination of the above two methods (Gill *et al.*, 1981). Therefore, it has the advantages of both methods, being fast and stable, and was chosen for this research.

5. Modeling Results

Before history-dependent simulation, we simulated Barbu *et al.*'s counter-current flow experiment (Barbu *et al.*, 1999) with the single p_c method. In this method, there is only one pair of relative permeability curves, which are represented in a power form using Equation (1). The single capillary pressure curve is constructed based on the final saturation profile using Equation (2). Figure 5(a) and (b) show the final match of the decane saturation profiles obtained by this method. The relative permeability and capillary pressure curves extracted by history-matching the saturation profiles of stage 2 were then used to model stage 1. Poor matches between the simulated and the experimental data are observed at the top of the sample in stage 1 (Figure 5(a)) and at the bottom of the sample in stage 2 (Figure 5(b)). These observations confirm the unsatisfactory matches shown in Figure 2. Application of the single p_c method to a thick formation may lead to significant errors in saturation profiles.

The history-dependent-modeling method was then used to simulate the same process. In this method, there are two pairs of relative permeability curves (drainage and imbibition), which are represented also with Equation (1). Each gridblock of the sample is assigned a distinct capillary pressure curve using Equations (3)–(6) according to the initial saturation and the local saturation history. Figure 6(a) and (b) show the final match of the saturation profiles from history-dependent simulation. Noticeable improvement in the upper part of the sample for stage 1 and the lower part for stage 2 can be seen compared to single p_c simulation (Figure 5(a) and (b)).

Figure 7 shows saturation distribution images from the experiment and the history-dependent simulation during stage 2. The simulation shows heterogeneous saturation distributions similar to the experimental findings and

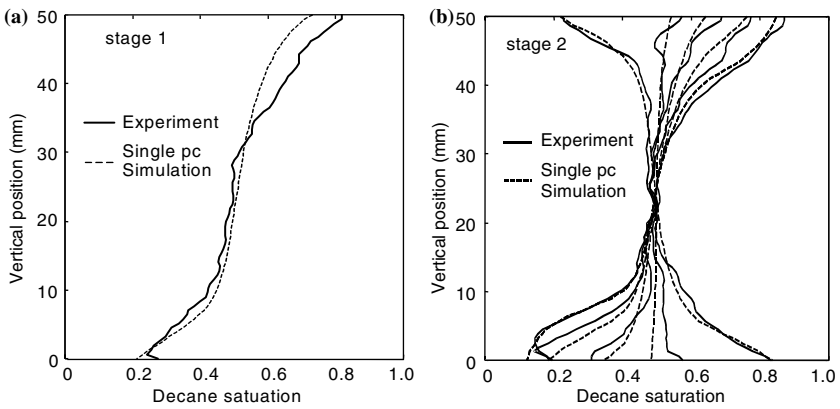

Figure 5. Decane saturation profiles of stage 1 and stage 2 in Barbu *et al.*'s experiment with single p_c simulation.

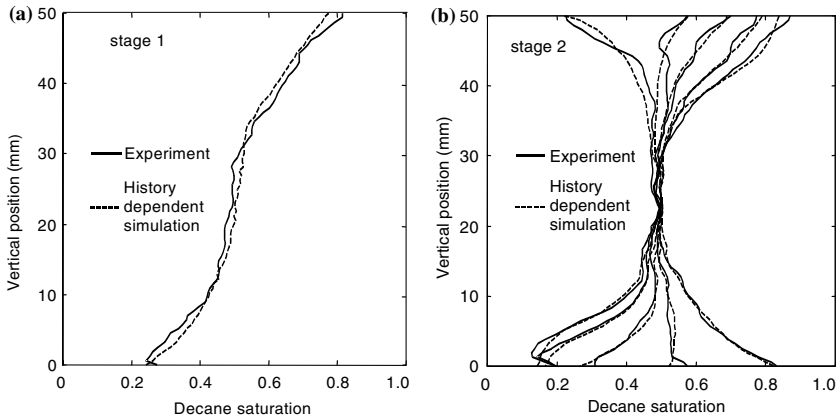

Figure 6. Decane saturation profiles of stage 1 and stage 2 in Barbu *et al.*'s experiment with history-dependent simulation.

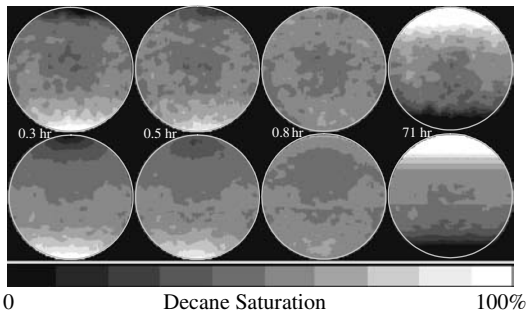

Figure 7. Comparison of saturation distribution between the experiment (top row) and the history-dependent simulation (bottom row).

there is no artifact from the influence of the round shape of the sample. This artifact is very strong when using the single p_c method (Figure 2), in which capillary pressure hysteresis is not taken into account. In the single p_c method, each grid block in the model uses the same capillary pressure curve, which acts like a filter and smoothes out the saturation variation. But in the history-dependent modeling, each grid block follows a different capillary pressure curve, which accounts for the local saturation history and preserves the saturation variation. The artifact caused with the single p_c method is consequence of the incorrect disregard for a fundamental mechanism in counter-current flow: the hysteresis.

6. Discussion

Earlier studies (Lenormand *et al.*, 1990; Al-Wadahi *et al.*, 2000) suggested that counter-current relative permeabilities are much smaller than

those of co-current flow. Kalaydjin (1990) attributed this relative permeability reduction to viscous coupling. Figure 8 shows the relative permeabilities obtained from different methods. The counter-current relative permeabilities obtained with the single p_c method (dotted line) are noticeably smaller than co-current relative permeabilities (solid line). The two pairs of relative permeability curves (drainage and imbibition) used in the saturation-history-dependent simulation are also smaller than the co-current relative permeabilities except for the case of the decane imbibition relative permeability.

Since the experiments modeled in the paper were done in closed systems, the following discussion is based on a closed system. For any pair of the relative permeability curves, only portions below cross points play a big role in the simulation. Portions above cross points are of limited contribution and fall into margin of large uncertainty. For this reason, the upper portions of the relative permeability curves including the end points cannot be accurately extracted from the experimental data. To explain this, a concept – total effective mobility needs to be introduced. In a closed system, the counter-current flow velocities of the heavy wetting phase and the light non-wetting phase are equal and given by the following equation (Templeton *et al.*, 1962):

$$v_{\mathrm{w}} = -v_{\mathrm{nw}} = \left(\frac{1}{\lambda_{\mathrm{w}}} + \frac{1}{\lambda_{\mathrm{nw}}}\right)^{-1} \left[\frac{dp_c}{dz} - (\rho_{\mathrm{w}} - \rho_{\mathrm{nw}})\, g\right] \tag{8}$$

where λ is mobility defined as the ratio of effective permeability of a fluid to its viscosity; subscript "w" represents wetting phase and "nw" represents non-wetting phase. The first term in the right hand side $\lambda_{te} = \left(\frac{1}{\lambda_{\mathrm{w}}} + \frac{1}{\lambda_{\mathrm{nw}}}\right)^{-1}$

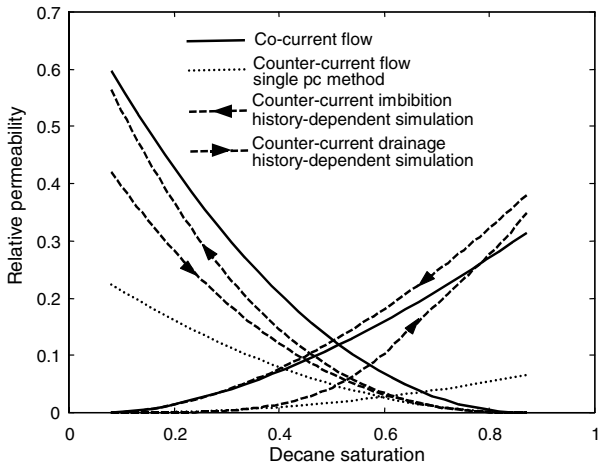

Figure 8. Relative permeabilities of Barbu *et al.*'s experiment.

represents the mobility of the system, which is defined as total effective mobility.

Total effective mobility represents the ability of fluids to flow through the system. This concept is valid for both co-current flow and counter-current flow from its derivation (Templeton *et al.*, 1962). From its definition, the total effective mobility is mainly controlled by the less mobile phase at any saturation, which corresponds to the small values of relative permeabilities below cross points in a closed system. The flow velocity in such a system is controlled by the total effective mobility and hence the relative permeabilities below cross points.

The capillary pressure hysteresis loop and the drainage and imbibition-scanning curves used in the current simulation are in Figure 9. The capillary pressure curve used in stage 1 is the thick solid curve. In stage 2, the lower part followed the dashed imbibition-scanning curves to the left and the upper part followed the dashed drainage-scanning curves to the right.

Figure 10 shows the capillary pressure hysteresis loop used in the saturation-history-dependent modeling and the capillary pressure curve used in the single p_c modeling. At low and high decane saturations, the capillary pressure curve in the single p_c method overlaps on the hysteresis loop and there is a transition zone in the middle. The curve in the transition zone is a combination of drainage and imbibition-scanning curves. This also explains why the capillary pressure curve used in single p_c simulation is "S"shaped.

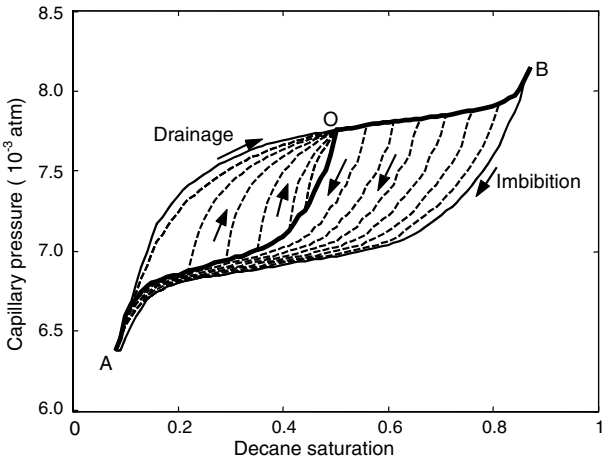

Figure 9. Capillary pressure hysteresis loop and scanning curves for Barbu *et al.*'s experiment used in history-dependent simulation.

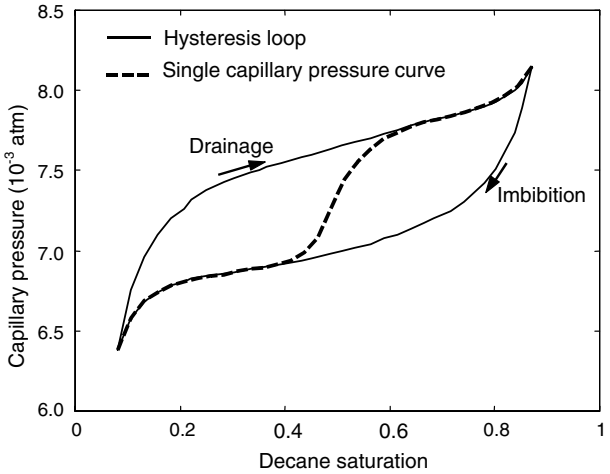

Figure 10. Capillary pressure curves of stage 2 in Barbu *et al.*'s experiment.

Compared to the single p_c method, history-dependent modeling is more physically sound, because it takes into account of the relative permeability and capillary pressure hysteresis. In the single p_c method, both the relative permeabilities and capillary pressures are the average parameters of history-dependent simulation. Therefore, the single p_c simulation only matches the average saturation profiles and it does not reproduce the details of the flow behavior of the system.

7. Conclusions

Based on the simulation of the counter-current flow experiment presented in this paper, the following conclusions may be drawn.

1. Relative permeability and capillary pressure hysteresis are essential for proper simulation of counter-current flow experiments. The single p_c method only produces the general behavior of a system and simulated saturation distributions are strongly affected by the shape of the sample.
2. The parameters used in the single p_c method are the average of the parameters used in history-dependent method. The relative permeabilities of single p_c method are smaller than those of history-dependent-modeling method. The S-shaped capillary pressure curve used in single p_c simulation is a combination of the drainage and imbibition-scanning curves.
3. Total effective mobility, mainly reflected by the relative permeabilities below cross points, controls the counter-current flow process in the simulated closed system.

References

Al-Wadahi, M., Grader, A. S. and Ertekin, T.: 2000, An Investigation of Three-Phase Counter-Current Flow Using X-Ray Computerized Tomography and Neuro-Simulation Modeling, *Proceedings*, SPE Annual meeting, Dallas, TX, USA.

Barbu, A., Hicks, P. J. and Grader, A. S.: 1999, Experimental three-phase flow in porous media: development of saturated structures dominated by viscous flow, gravity, and capillarity, *SPE J*. December.

Briggs, J. E. and Katz, D. L.: 1966, Drainage of Water from Sand in Developing Aquifer Storage, *Proceedings*, SPE Annual Meeting, Dallas, TX, USA.

Everett, D. H.: 1967, Adsorption hysteresis, in: E.A. Flood (ed.), *The Solid–Gas Interface*, Vol. 2, Chapter 36, Mercel, New York. p. 1055.

Gill, P. E., Murray, W. and Wright, M. H.: 1981, *Practical Optimization*, Academic Press, New York.

Killough, J. E.: 1976, Reservoir simulation with history-dependent saturation functions, *SPE J.* February.

Kleppe, J., Delaplace, P., Lenormand, R., Hamon, G. and Chaput, E.: 1997, Representation of Capillary Pressure Hysteresis in Reservoir Simulation, *Proceedings*, SPE Annual Meeting, San Antonio, TX, USA.

Lenormand, R., Kalaydjin, F., Bieber, M. T. and Lombard, J. M.: 1990, Use of a Multifractal Approach for Multiphase flow in Heterogeneous Porous Media: Comparision with CT-Scanning Experiment, *Proceedings*, SPE Annual Meeting, New Orleans, LA, USA.

Morrow, N. R. and Harris, C. C.: 1965, Capillary equilibrium in porous materials, *SPE J*. March.

Morrow, N. R.: 1970, Physics and thermodynamics of capillary, in: (edited by ACS) *Flow Through Porous Media*, Washington, DC.

Philip, J. R.: 1964, Similarity hypothesis for capillary hysteresis in porous materials, *J. Geophys. Res.* **69** (8).

Poulovassilis, A.: 1962, Hysteresis of pore water, an application of the concept of independent domains, *Soil Sci.* **93**, 405.

Templeton, E. E., Nielsen, R. F. and Stahl, C. D.: 1962, A study of gravity counterflow segregation, *SPE J*. June.